SUPPLEMENTAL MATERIAL

Body Surface Localization of Left and Right Atrial High Frequency Rotors in Atrial Fibrillation Patients: A Clinical-Computational Study

Heart Rhythm: In Press Accepted Manuscript (published online May 17, 2014)

Body Surface Localization of Atrial Rotors

Miguel Rodrigo, M.S.[1], María S Guillem, Ph.D.[1], Andreu M Climent, Ph.D. [2], Jorge Pedrón-Torrecilla, M.S.[1], Alejandro Liberos, M.S.[1], José Millet, Ph.D.[1], Francisco Fernández-Avilés, M.D., Ph.D.[2], Felipe Atienza, M.D.,Ph.D.[2], Omer Berenfeld, Ph.D., F.H.R.S. [3]

[1] Bio-ITACA, Universitat Politécnica de Valencia, Valencia, Spain

[2] Cardiology Department, Hospital General Universitario Gregorio Marañón, Instituto de Investigación Sanitaria Gregorio Marañón, Madrid, Spain

[3] Center for Arrhythmia Research, University of Michigan, Ann Arbor, U.S.A.

Address for correspondence: Maria S. Guillem, ITACA, Universidad Politécnica de Valencia, Camino de Vera sn, 46022 Valencia (Spain), tel.: +34963877968, email: mguisan@eln.upv.es or Felipe Atienza, Cardiology department, Hospital General Universitario Gregorio Marañón, C/ Dr Esquerdo 46, 28007, Madrid (Spain), tel.: +34915868281, email: fatienza@secardiologia.es.

METHODS

Patients and body surface potential recording

Surface electrocardiograms (ECGs) were recorded simultaneously to intracardiac electrograms (EGMs) on 14 patients using a grid of 67 electrodes on a vest covering the torso distributed as follows: 28 electrodes on the anterior, 34 on the posterior and 2 on each lateral side of the torso (Fig. S1A). Three limb leads were also recorded to obtain a Wilson Central Terminal. The signals were recorded using a commercial system (Active Two, Biosemi, The Netherlands) at a sampling frequency of 2048 Hz and were stored for off-line analysis. A central venous bolus of adenosine (12-18 mg) was administered in order to produce a significant atrio-ventricular block and to remove the ventricular activation [1]. At peak adenosine effect, the 67 surface ECGs were recorded and a 4-seconds segments surrounding the longest RR interval was used for the analysis. In cases with ventricular activation pauses shorter than 4 seconds, the QRST were cancelled [2].

Surface potentials were processed using Matlab 7.10.0 (The Mathworks Inc, Natick, MA). Recorded ECG signals properly arranged in space were used to estimate ECG signals at non-recorded positions using cubic spline interpolation [3]. Baseline was estimated by decimation to 51.2 Hz and filtering with a Butterworth 10th-order low-pass filter with a cut-off frequency of 2 Hz. This signal was interpolated to 2048 Hz and subtracted from the original signal [3]. Leads presenting >0.5% of their spectral content at 50Hz were filtered with a second-order infinite impulse response notch filter centered at 50 Hz. Potential signals were low-pass filtered with a 10th-order Butterworth filter with a cut-off frequency of 30 Hz. All leads were visually inspected after filtering and leads with noticeable noise were excluded from further analysis. Power spectral density of all signals free of ventricular activity was computed using Welch periodogram (2-second Hamming window with an 8192 point Fast Fourier transform per window and 50% overlap) to determine the local DFs and their distribution on the body surface.

Surface ECGs were then filtered at the highest DF (HDF) found on the torso surface or at the highest DF found at either left atrium EGMs (LA-HDF) or right atrium EGMs (RA-HDF) by using a cascade of a high-pass Chebyshev 10th order filter with cut-off frequency equal to HDF - 1 Hz and a low-pass 10th order Chebyshev filter with a cut-off frequency equal to HDF + 1 Hz after decimation of ECG signals down to a sampling frequency of 128 Hz.

Computational models of the atria and torso

The active tissue of the atria consisted of a 2.5 cm radius sphere incorporating 163,842 nodes (average inter-nodal distance of 236,07 ± 15.35 μm) on which the transmembrane potential kinetics ionic formalism [4-5] was used. The system of differential equations was solved by using Runge-Kutta integration with an adaptive temporal step based on a graphic processors unit (NVIDIA Tesla C2075 6G) [6]. All signals were re-sampled at sampling frequency of 1 kHz.

Three atrial tissue types were used to construct different propagation patterns: Right atrium (RA) tissue, left atrium (LA) tissue and fibrotic tissue. The LA and RA tissues were modeled by setting the $I_{K,ACh}$ and I_{Kr} conductances to 2 and 1.6 fold, respectively in the LA relative to the RA [1]. Fibrotic tissue was modeled by simply disconnecting 57% of nodes in the RA tissue. Three propagation patterns were simulated on the atrial sphere: (1) a sphere was divided into a LA hemisphere that harbored a stable functional rotor and a RA hemisphere with fibrillatory activity driven by the LA rotor (Figure 2 and Figure S2); (2) a sphere divided into a LA hemisphere that harbored a stable rotor and another hemisphere with fibrotic conduction (Figure 3 and Figure S4) and (3) a sphere in which only 5% to 30% of the surface had LA properties and harbored a stable rotor and the remaining surface of the sphere presented fibrotic properties (Figure S3).

The electric potential resulting from the wave propagation simulated on the atrial sphere was studied everywhere on 20 concentric spheres of 2562 nodes with increasing radii from 2.5 cm to 12.5 cm. In order to obtain the electric potential, the forward problem formalism was solved by using the Boundary Element Method [7]. The potentials on the external sphere, defined as the torso surface, and in the internal layers were analyzed to characterize the time-course of the potential distribution everywhere; in particular, the patterns and time-course of the filaments resulting from rotors in the atria were characterized.

Phase singularity and filaments

To increase reliability, the phase values were obtained along 3 different circles surrounding each evaluated point; an evaluated point was defined as a SP only when the phases of at least two of these three circles was gradually and monotonically increasing or decreasing for a total of 2π.

In patients, the radii of the circles used for evaluating SPs were 1.66%, 3.31% and 5.53% respectively of the individual patient's torso circumference. SPs in consecutive time instants were considered to be related, i.e., belong to the same rotor, if they maintained a continuity of rotation and were separated by <5.53% of the patient's torso circumference. Functional rotors were defined as related SPs that complete at least one turn.

In the computational models, the radii of the circles used for detecting SPs were of 0.08·R, 0.15·R and 0.2·R, where R was the radius of the layer (1, 1.8 and 2.5 cm at the outermost layer). A filament was defined as the connection between SPs across spherical layers at a given time. Specifically, two SPs in different layers were connected to construct a filament when the distance between these SPs was less than 0.4·R. Additionally, the distance between SPs at any layer in consecutive time instants

should be less than 0.4·R to be related and maintain a continuity of rotation. Finally, only long lasting filaments, defined as those that complete at least one rotation on the outermost surface, were considered as rotors and all other filaments were discarded.

RESULTS

Surface mapping of organized atrial activation

As an initial step in our study we studied sample surface phase maps recorded from a patient during a typical atrial flutter (Figure S1B). The surface activation during atrial flutter should represent organized patterns which have a direct correlation with the propagation sequence in the atria and should serve as a reference for further, more complex patterns of atrial activation during AF. Three sequential phase maps during the sample atrial flutter recorded with our surface electrodes grid show a rotational activity with a stable pattern (Figure S1B). Two SPs appear on the surface phase maps most likely corresponding to a single anatomical reentry, as discussed in Figure S2 and elsewhere in the manuscript.

Simulations to understand HDF band-pass filtering of AF patterns

Smallest reentry detected on the surface. Figure S3 demonstrates that the ability of surface potentials to detect SPs may depend on the amount of tissue activated around the SP. In Figure S3 we analyze a model with a reduced driving rotor area; the spherical atria is divided into a 10% LA area and 90% fibrotic area and the filament originating at the simulated stable LA rotor is not stable at the surface (Figure S3A-B). Following HDF filtering the filament originating at that driving rotor reaches the surface at the nearest point from the epicardial SP and remains stable over time together with its mirror rotor, as can be observed in Figure S3B-C. In our simulations, HDF filtering was required in order to detect the “true” SP in simulations for fibrotic tissue covering more than 80% of the atrial surface. Without HDF filtering, detected SPs where unstable: they were not present all of the time and had short-lasting durations (Figure S3D).

Effect of torso volume inhomogeneity in surface phase maps

Our multi-spherical model assumes certain simplifications of the electrical propagation problem between atria and torso, as considering atria and torso as spheres or the homogeneity of the electrical properties of the torso volume. In order to study the effect of the inhomogeneity of the torso volume, we simulated the electrical propagation of the atrial activity also under inhomogeneity volume properties. In particular, we evaluated the effect of subvolumes with a 2.2 fold reduction of electrical conductivity, simulating the lungs, on the surface potentials (Figure S4). In Panel A, we can notice that insertion of lungs alter the phase map on the torso surface, although the deflection of phase singularities is subtle.

REFERENCES

1. Atienza F, Almendral J, Moreno J, et al: Activation of inward rectifier potassium channels accelerates atrial fibrillation in humans: evidence for a reentrant mechanism. Circulation 2006; 114:2434–2442.

2. Castells F, Mora C, Rieta JJ, Moratal-Pérez D, Millet J. Estimation of atrial fibrillatory wave from single-lead atrial fibrillation electrocardiograms using principal component analysis concepts. Med Biol Eng Comput 2005; 43:557–560.

3. Guillem MS, Climent AM, Castells F, Husser D, Millet J, Arya A, Piorkowski C, Bollmann A: Noninvasive mapping of human atrial fibrillation. J Cardiovasc Electrophysiol 2009; 20:507–513.

4. Courtemanche M, Ramirez RJ, Nattel S: Ionic mechanisms underlying human atrial action potential properties: insights from a mathematical model. Am J Physiol 1998; 275:301-321.

5. Kneller J, Zou R, Vigmond EJ, Wang Z, Leon LJ, Nattel S: Cholinergic atrial fibrillation in a computer model of a two-dimensional sheet of canine atrial cells with realistic ionic properties. Circ Res 2002; 90:73-87.

6. García VM, Liberos A, Vidal AM, Guillem MS, Millet J, González A, Martinez-Zaldivar FJ, Climent AM: Adaptive step ODE algorithms for the 3D simulation of electric heart activity with graphics processing units. Computers in Biology and Medicine (in press, DOI information: 10.1016/j.compbiomed.2013.10.023).

7. Horácek BM, Clements JC: The inverse problem of electrocardiography: a solution in terms of single- and double-layer sources of the epicardial surface. Math Biosci 1997; 144:119-154.

Table 1. Patient's characteristics

N	14
Age Range	56 ± 8 years 47-68 years
Gender - male	13 (93%)
Years since AF diagnosis Range	5 ± 4 years 1-17 years
AF type - paroxysmal	10 (71%)
# of previous ablations Range	1 ± 1 0-3
DF gradient in EGMs	12 (86%)

Figure legends

Figure S1. Surface phase maps during organized atrial rhythms. (A) Schematic geometrical configuration of the surface electrodes relative to the torso. Circles represent the location of recording electrodes. Electrodes at locations corresponding to the standard ECG precordial leads are denoted as black circles. (B) Surface phase maps during typical atrial flutter at three selected time instants. Red dots superimposed on V1 tracings indicate the time instants selected for phase maps representation.

Figure S2. Illustration of the concept of true and mirror rotor filaments. The figure shows two opposing viewpoints of a simulated activity in a model that includes atrial tissue, torso volume and torso surface. Atrial voltage maps are represented according to a color scale from blue to red (color bar scale). The atrial activity consists of a stable and fast LA rotor with a fixed SP and an unstable wavebreak with unstable SP at the interface of the LA hemisphere with the slower activity at the RA hemisphere (see also Figure 2). Upon band-pass filtering of the surface data at the frequency of the stable LA rotor, two stable reentries (red wavefont patterns on the surface of the torso are the pivoting rotors with the chirality indicated by the circular arrows) with two fixed SPs become visible on the torso surface; one is termed the true SP and the other the mirror SP, based on the trajectory of the filament connecting them with the source atrial rotor. The true SP is connected to the source rotor directly (green filament) and the mirror SP is connected to the source rotor intersecting the contralateral atrial wall (blue filament), where no stable rotor at the frequency of the LA rotor is present (see rear view panel on the right side).

Figure S3. Epicardial and transition to surface phase maps during AF in a 10 % LA – 90 % fibrosis atrial model. (A) Phase maps at 4 time instants (top to down) in 3 concentric layers at increasing distances from the epicardium (left to right) and after HDF filtering of surface potentials. (B) Phase map of epicardial sphere and temporal evolution of filaments for unfiltered potentials and for HDF-filtered potentials. (C) Transmembrane potential at the epicardial sphere with tracking of intracardiac (red) and surface (black) rotors after HDF filtering. (D) Percentage of time with rotors and maximum rotor duration in surface phase maps from unfiltered and HDF-filtered potentials for increasing sizes of the fibrotic tissue.

Figure S4. Surface phase maps during AF in a 50 % LA – 50 % fibrosis atrial model with an inhomogeneous torso model including lungs. (A) Location of lungs inside the torso volume. Lungs were simulated as two spheres with 7.5 cm of diameter placed between atria and torso. (B) Phase maps at 3 time instants (left to right) at the torso sphere in homogeneous torso model (no lungs) and in the inhomogeneous torso model (with lungs). (C) Transmembrane potential at the epicardial sphere with tracking of intracardiac (red) and surface rotors from the homogeneous torso model (black) and at the inhomogeneous torso model (green).

Movie 1. Movie showing consecutive phase maps and rotor tracking after LA-HDF filtering in an LA-fastest patient (Figure 5A). The movie shows a detected rotor that lasted for 2 s.

Movie 2. Movie showing consecutive phase maps and rotor tracking after RA-HDF filtering in an RA-fastest patient (Figure 5B). The movie shows a detected rotor that lasted for 500 ms.

FIGURE S1

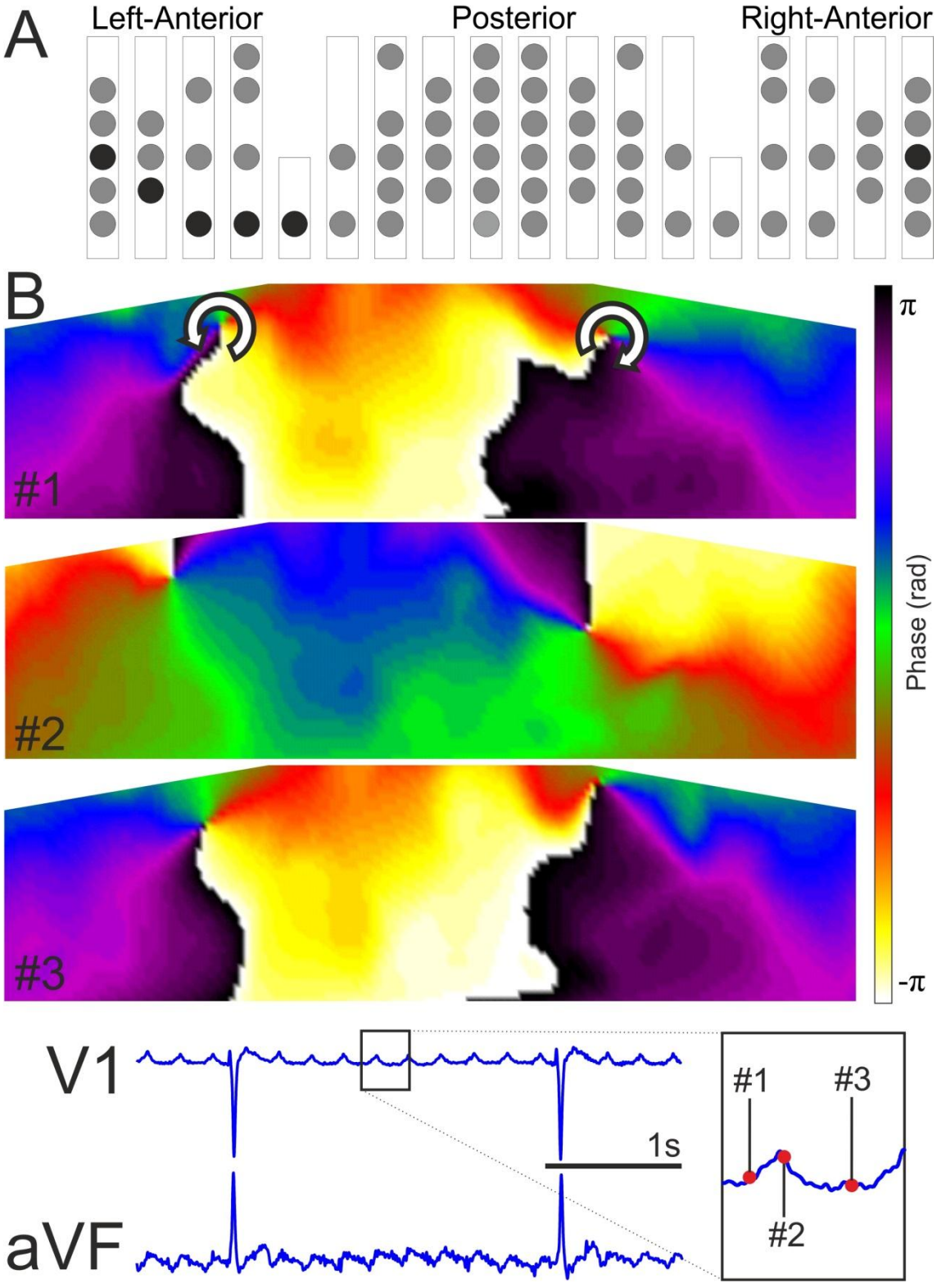
A
Left-Anterior
Posterior
Right-Anterior
B
#1
#2
#3
π
Phase (rad)
-π
V1
aVF
1s
#1
#3
#2

FIGURE S2

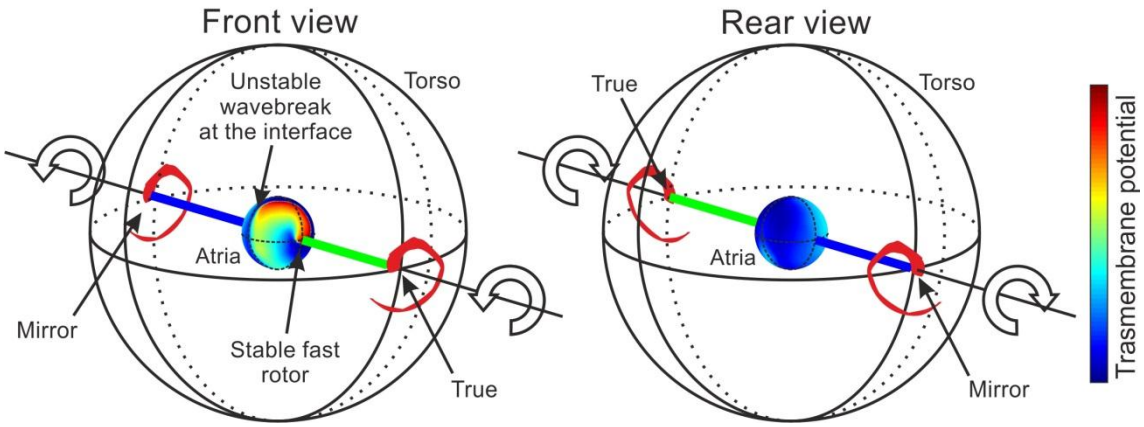
Front view
Unstable
wavebreak
at the interface
Torso
Atria
Mirror
Stable fast
rotor
True
Rear view
True
Torso
Atria
Mirror
Trasmembrane potential

FIGURE S3

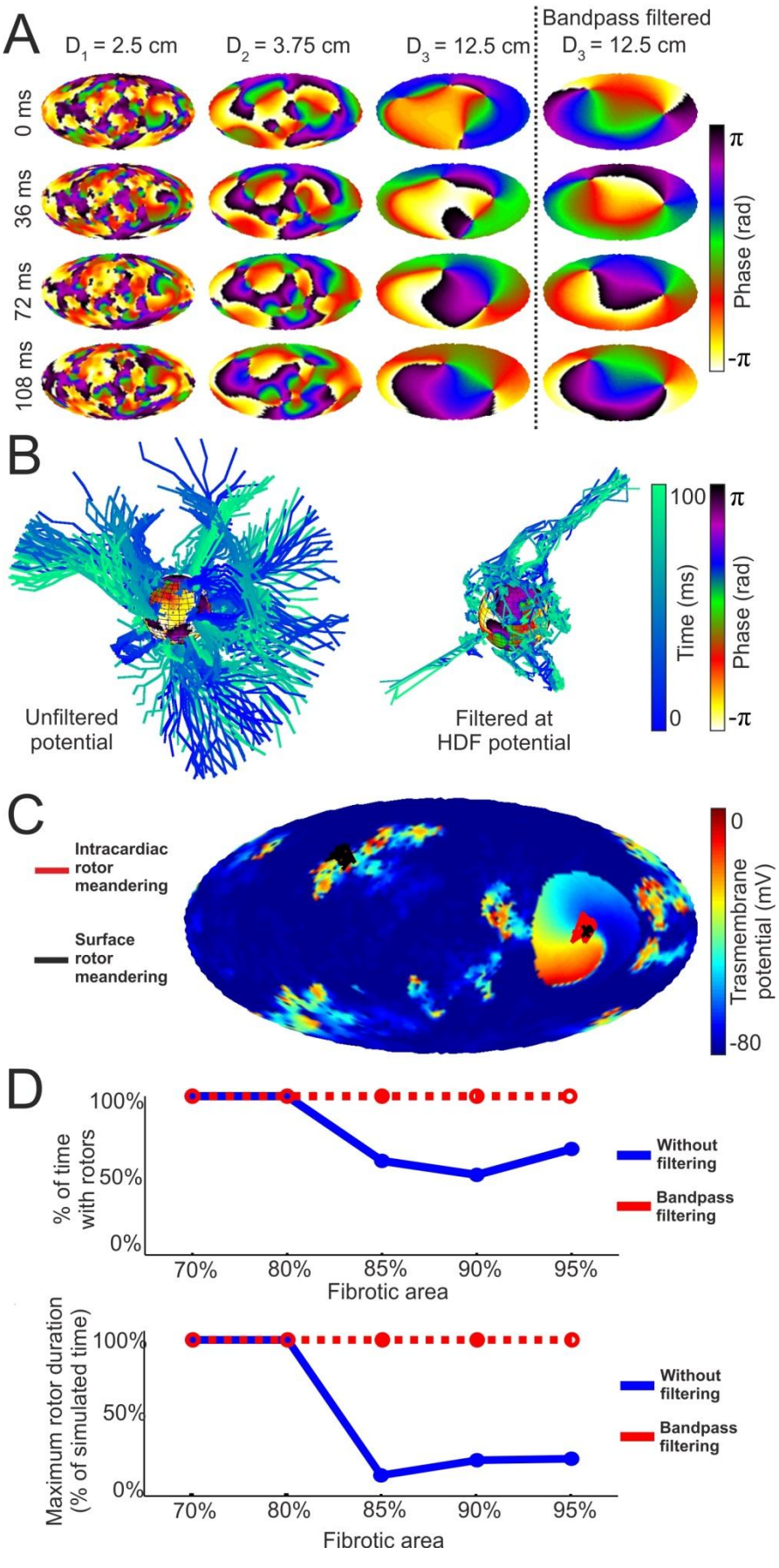
A
D1 = 2.5 cm
D2 = 3.75 cm
D3 = 12.5 cm
Bandpass filtered
D3 = 12.5 cm
0 ms
36 ms
72 ms
108 ms
π
Phase (rad)
-π
B
Unfiltered potential
Filtered at HDF potential
100
Time (ms)
0
π
Phase (rad)
-π
C
Intracardiac rotor meandering
Surface rotor meandering
0
Trasmembrane potential (mV)
-80
D
100%
50%
0%
% of time with rotors
70%
80%
85%
90%
95%
Fibrotic area
Without filtering
Bandpass filtering
Maximum rotor duration (% of simulated time)
100%
50%
0%
70%
80%
85%
90%
95%
Fibrotic area
Without filtering
Bandpass filtering

FIGURE S4

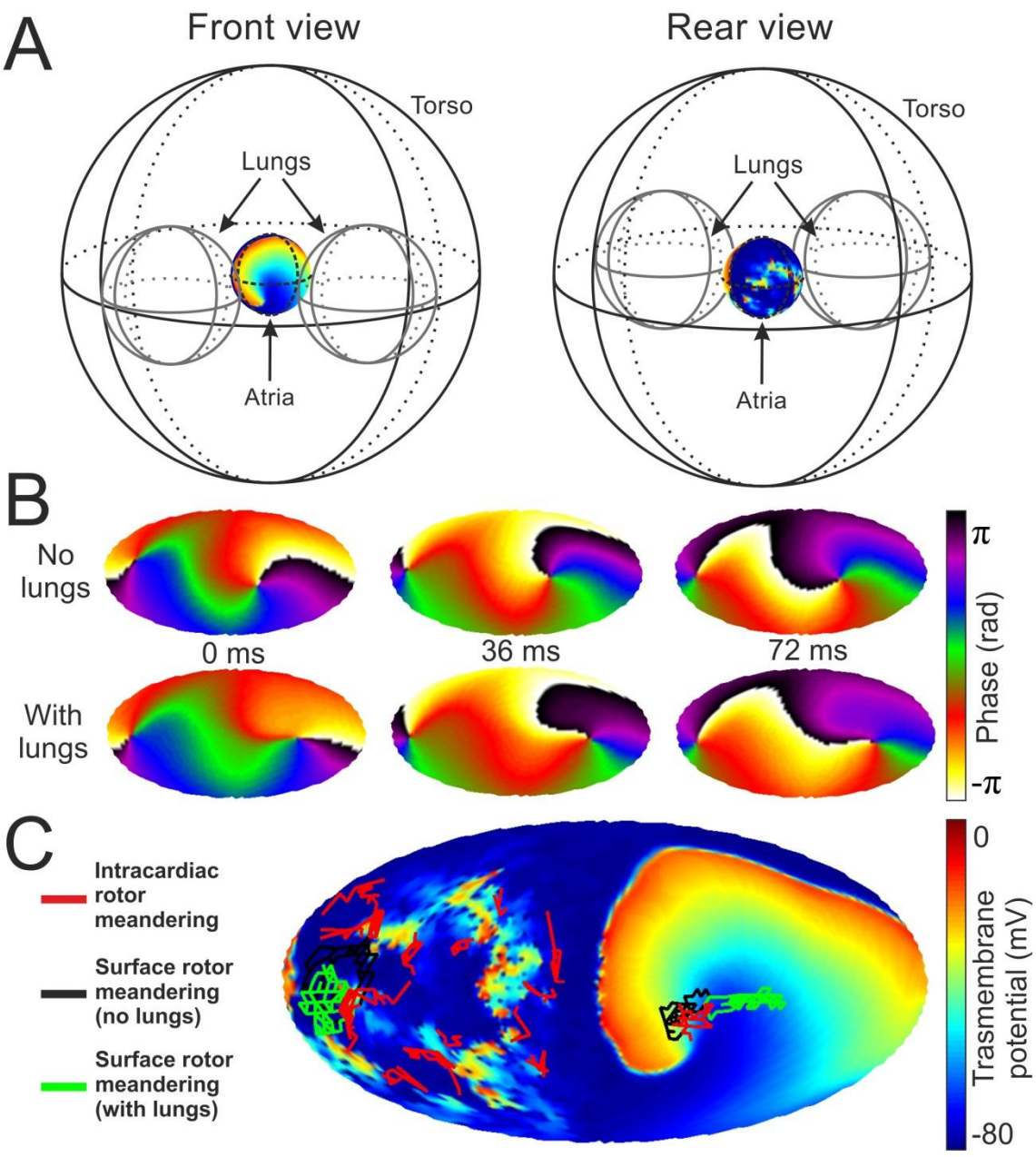
A
Front view
Rear view
Torso
Lungs
Atria
Torso
Lungs
Atria
B
No lungs
With lungs
0 ms
36 ms
72 ms
π
Phase (rad)
-π
C
Intracardiac rotor meandering
Surface rotor meandering (no lungs)
Surface rotor meandering (with lungs)
0
Trasmembrane potential (mV)
-80